AD-A072 827 ATMOSPHERIC SCIENCE ASSOCIATES BEDFORD MASS F/G 4/1
COLLECTION AND MEASUREMENT EFFICIENCIES OF THE EWER CLOUD WATER--ETC(U)
MAY 79 H G NORMENT F19628-79-M-0005

UNCLASSIFIED AFGL-TR-79-0122 NL

1 OF 1
AD A072827

END
DATE FILMED
9-79
DDC

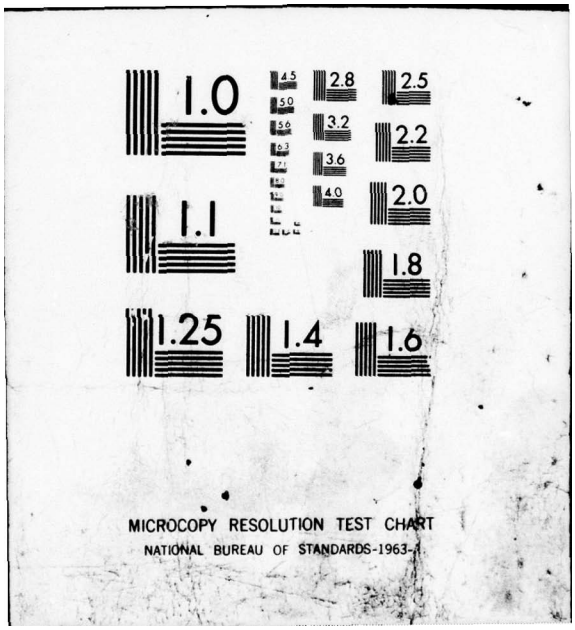
1.0
1.1
1.25
1.4
1.6
1.8
2.0
2.2
2.5
2.8
3.2
3.6
4.0
4.5
5.0
5.6
6.3
MICROCOPY RESOLUTION TEST CHART
NATIONAL BUREAU OF STANDARDS-1963-A

LEVEL II (12)

AFGL-TR-79-0122

COLLECTION AND MEASUREMENT EFFICIENCIES OF THE EWER CLOUD WATER METER FOR HYDROMETEORS

Hillyer G. Norment

Atmospheric Science Associates
363 Great Road
P.O. Box 307
Bedford, Massachusetts 01730

11 May 1979

Final Report
1 April 1979 - 31 May 1979

Approved for public release; distribution unlimited

AIR FORCE GEOPHYSICS LABORATORY
AIR FORCE SYSTEMS COMMAND
UNITED STATES AIR FORCE
HANSCOM AFB, MASSACHUSETTS 01731

UNCLASSIFIED

SECURITY CLASSIFICATION OF THIS PAGE (When Data Entered)

REPORT DOCUMENTATION PAGE

READ INSTRUCTIONS BEFORE COMPLETING FORM

1. REPORT NUMBER (18) AFGL-TR-79-0122 (19)

2. GOVT ACCESSION NO.

3. RECIPIENT'S CATALOG NUMBER

4. TITLE (and Subtitle) (6)
COLLECTION AND MEASUREMENT EFFICIENCIES OF THE EWER CLOUD WATER METER FOR HYDROMETEORS

5. TYPE OF REPORT & PERIOD COVERED (9)
1 April 79 - 31 May 79
Final rept.

6. PERFORMING ORG. REPORT NUMBER
1 apr-31 May 79

7. AUTHOR(s) (10)
Hillyer G. Norment

8. CONTRACT OR GRANT NUMBER(s) (15)
F19628-79-M-0005

9. PERFORMING ORGANIZATION NAME AND ADDRESS
ATMOSPHERIC SCIENCE ASSOCIATES
363 Great Road, P. O. Box 307
Bedford, MA 01730

10. PROGRAM ELEMENT, PROJECT, TASK AREA & WORK UNIT NUMBERS
(16) P.E. 61102F
2310 G5 01 (17) G5

11. CONTROLLING OFFICE NAME AND ADDRESS (11)
Air Force Geophysics Laboratory (LYC)
Hanscom AFB, Massachusetts 01731
Contract Manager: Mr. Wilbur Paulsen

12. REPORT DATE
11 May 1979

13. NUMBER OF PAGES
38

14. MONITORING AGENCY NAME & ADDRESS (if different from Controlling Office)
(12) 39p.

15. SECURITY CLASS. (of this report)
Unclassified

15a. DECLASSIFICATION/DOWNGRADING SCHEDULE

16. DISTRIBUTION STATEMENT (of this Report)
Approved for publication; distribution unlimited

17. DISTRIBUTION STATEMENT (of the abstract entered in Block 20, if different from Report)

18. SUPPLEMENTARY NOTES

19. KEY WORDS (Continue on reverse side if necessary and identify by block number)
cloud physics
water drop concentration
ice crystal concentration
Research Aircraft
EWER
Calibration of airborne hydrometeor samplers

20. ABSTRACT (Continue on reverse side if necessary and identify by block number)
Calculated collection and measurement efficiencies for an airborne EWER cloud water content meter are presented for water drops and five types of ice crystals for three flight altitudes and for wide ranges of particle sizes. Particle type and size effects are found for very small particles, but the results are essentially constant for particles heavier than about 0.5 μg.
MICROGRAMS

DD FORM 1 JAN 73 1473 EDITION OF 1 NOV 65 IS OBSOLETE

Unclassified

SECURITY CLASSIFICATION OF THIS PAGE (When Data Entered)

392 152

4/B

TABLE OF CONTENTS

LIST OF FIGURES

LIST OF TABLES

INTRODUCTION

The Meteorology Division, Air Force Geophysics Laboratory, operates an MC130E cloud physics research airplane which is outfitted with a variety of instruments to measure hydrometeor concentrations aloft. An important application of this research airplane is to determine concentrations of hydrometeors which could cause missile erosion.

The instrument of concern here is called the EWER (Evaporation of Water that Erodes on Reentry) which measures hydrometeor water content. It is provided with a relatively large intake aperature (10 cm^2), so to adequately sample low concentrations of hydrometeors, which is analogous to the wide mouth of a ewer jar.

Calculated collection and measurement efficiencies of the EWER are reported here for water drops and five types of ice hydrometeors over wide ranges of particle sizes and flight conditions.

EWER DESCRIPTION

In external appearance the EWER consists of a pair of tapered tubes (probes) protruding from the forward end of the left-hand wing pod on the MC130E airplane (Fig. 1). Details of its development, construction and calibration are given by Durran, et al.[1] Figure 2 shows critical dimensions.

A schematic which illustrates operation of the instrument is shown in Fig. 3. In the reference probe hydrometeors are separated from the flow such that only moist air passes through to the detector. Air and hydrometeors are allowed to pass through the main probe, but they are heated such as to vaporize all water. Water content (mass of water per unit volume of air) is derived from light attenuation by the water vapor which passes through the detector. The detector consists of four Lyman-α humidometers mounted on a rotating head such that each humidometer in turn samples both the total and reference water vapor. The reference water vapor content is subtracted from the total water vapor content to yield the hydrometeor water content.

Air sampling by the EWER is not isokinetic. Air sampling efficiency, η (airflux into the EWER divided by free stream air flux), is shown in Fig. 4 as a function of flight (i.e., free stream) airspeed. For our calculations we have taken η to be 0.45.

---

1. D. A. Durran, D. H. Ross and W. J. Swartwood, "Development of Cloud Water Content Meter, EWER," The Aerospace Corp., Report SAMSO-TR-78-113 (March 1978). AD-A061 255

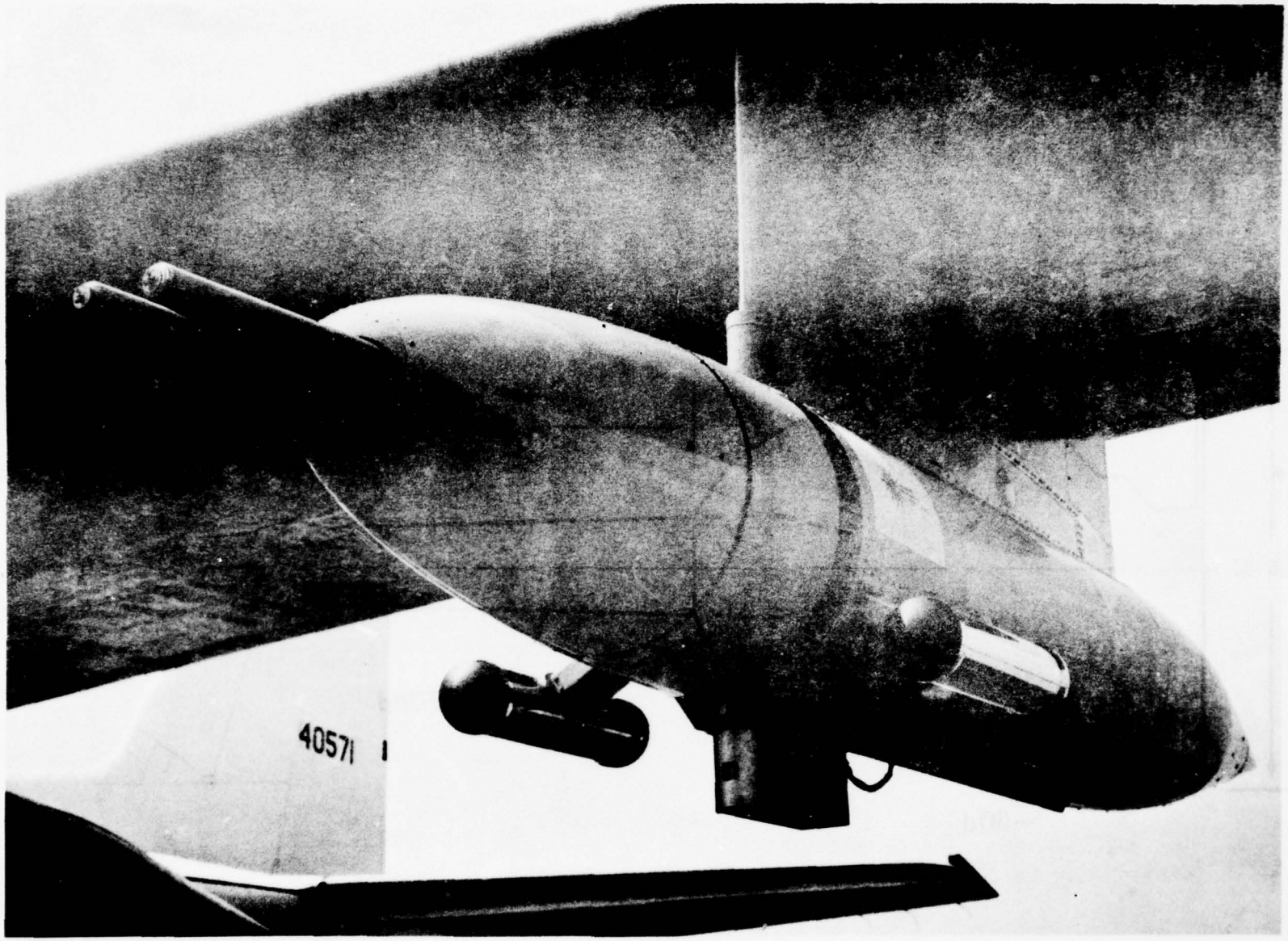

Figure 1. Wing pod and EWER mounted under the left wing on the MC130E.

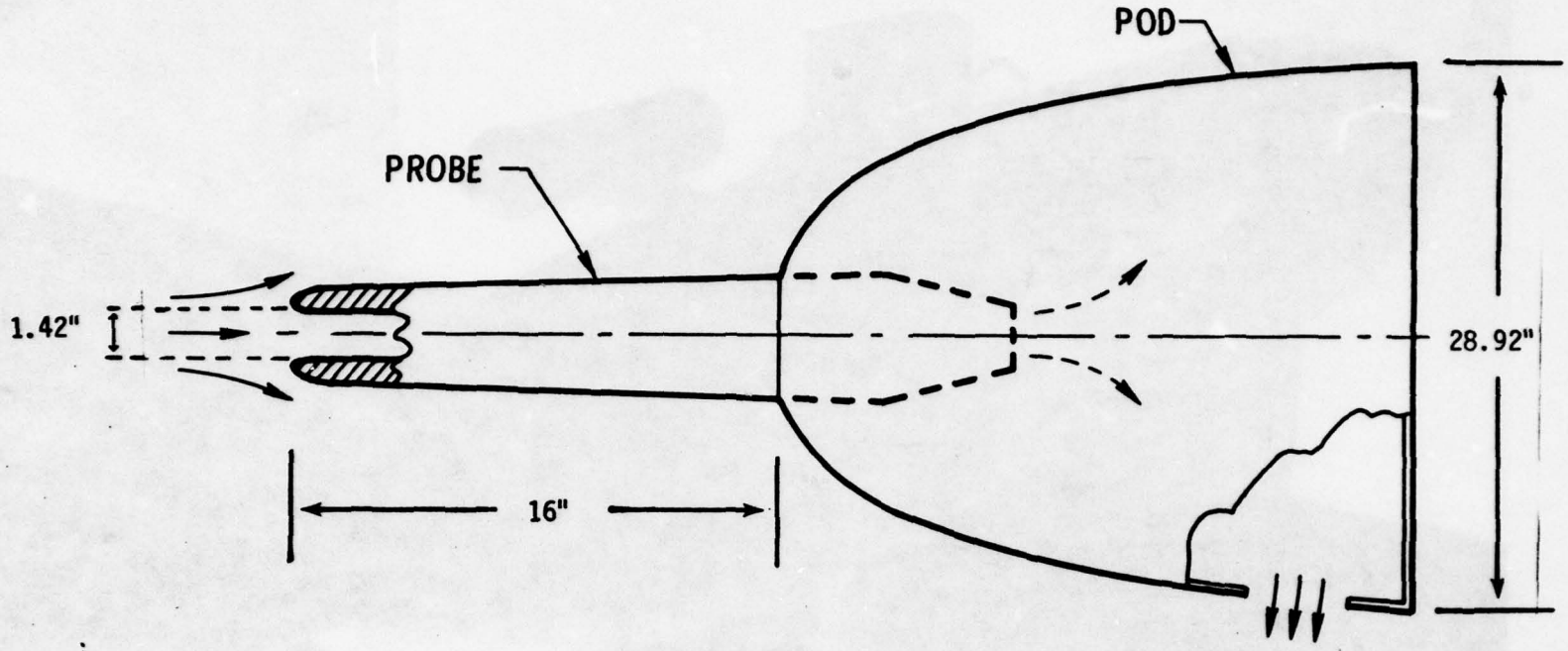

Figure 2. Side-view of the EWER probe and wing pod nose.
(From Durran, et al.[1])

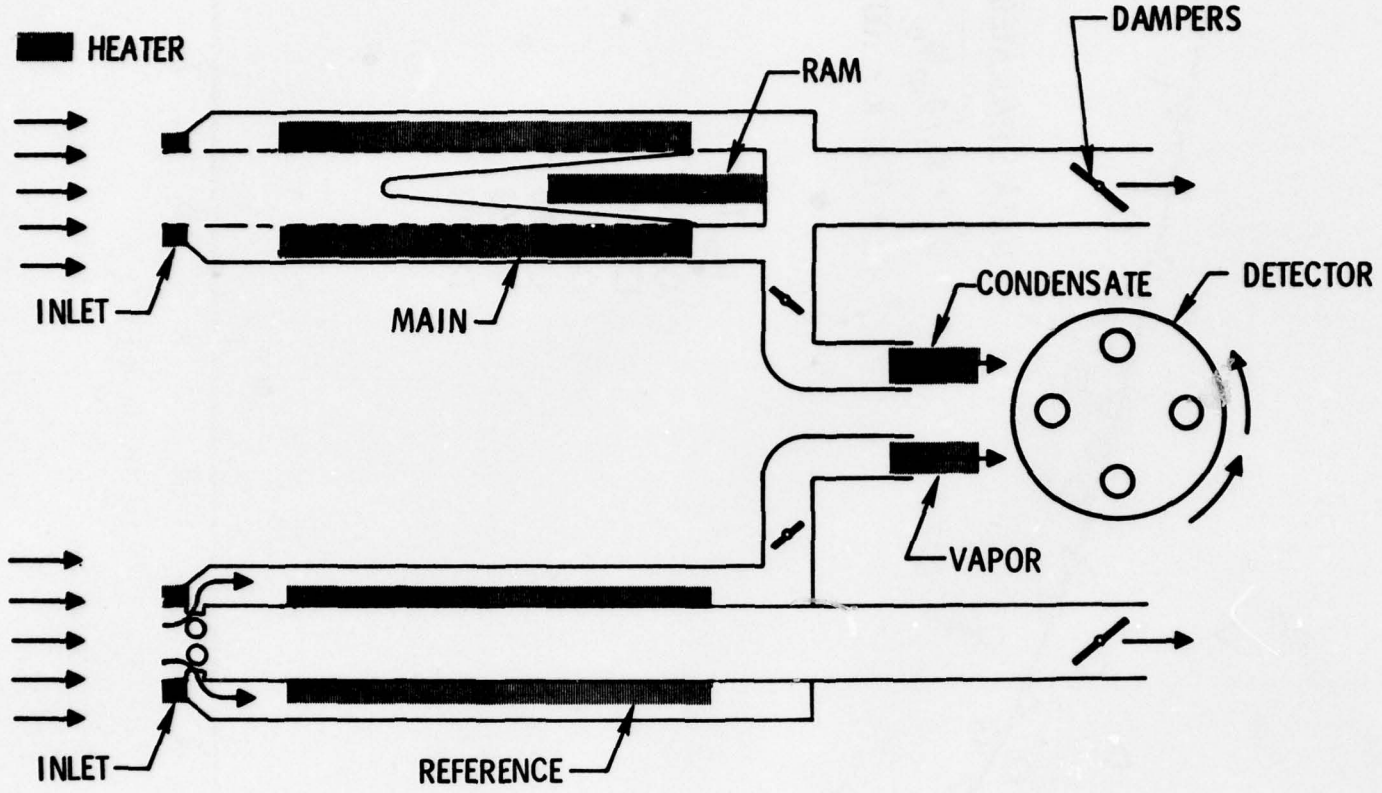

Figure 3. EWER Schematic. (From Durran, et al.[1])

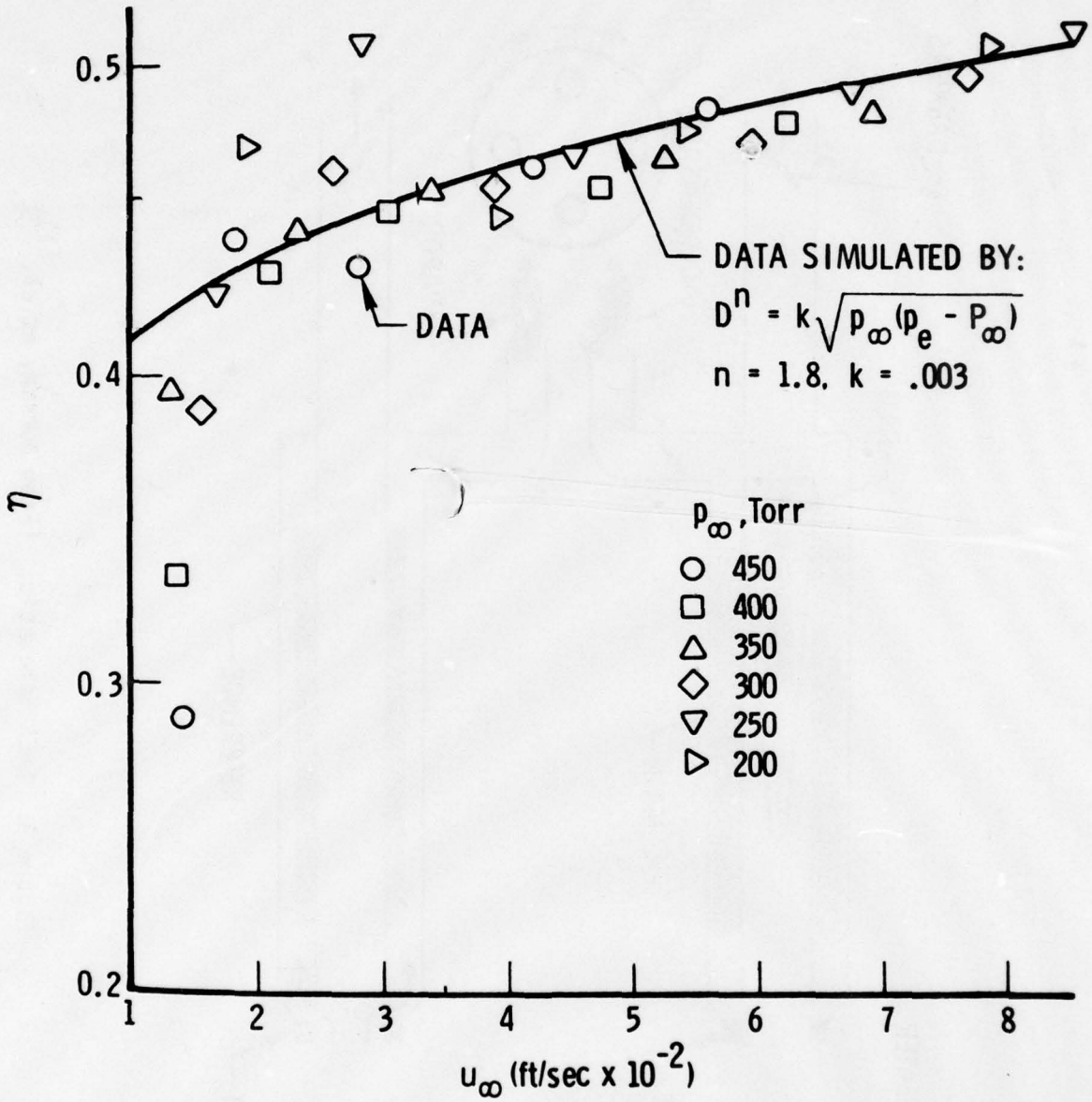

Figure 4. Air intake efficiency vs. flight parameters for the EWER. (From Durran, et al.[1])

COLLECTION AND MEASUREMENT EFFICIENCY CALCULATIONS

GENERAL DISCUSSION

The EWER probes are mounted far enough from the airplane wing, propellers and fuselage that their orifices are essentially in the free stream. However, as noted above air sampling is at about 45% of the free stream flux under normal flight conditions. Since partial stagnation occurs at the orifices, the question arises as to how this affects hydrometeor sampling and measurement.

To calculate collection efficiency, we develop a digital description of the EWER probes and wing pod nose and use this to calculate air flow around and into the EWER orifices for specified flight conditions. Then we compute trajectories of hydrometeors through the three-dimensional flow field from the undisturbed cloud into the orifices such as to define a quantity called concentration factor.[2,3,4]

Concentration factor, C_F, is defined as the ratio of particle flux at the sampling or target point, F_t, to the particle flux in the free stream, F,

$$C_F \equiv \frac{F_t}{F} \quad . \tag{1}$$

Concentration ratio, $C_{M,t}$, is the ratio of the particle concentration at the target point to free stream concentration,

$$C_{M,t} = C_F \, V/V_{p,t} \quad , \tag{2}$$

where $V_{p,t}$ is the particle speed into the orifice and V is free stream airspeed.

2. H. G. Norment and R. G. Zalosh, "Effects of Airplane Flowfields on Hydrometeor Concentration Measurements," AFCRL-TR-74-0602 (6 Dec. 1974) AD-A006 690
3. H. G. Norment, "Effects of Airplane Flowfields on Cloud Water Content Measurements," AFCRL-TR-75-0231 (30 April 1975). AD-A014 807
4. H. G. Norment, "Additional Studies of the Effects of Airplane Flowfields on Hydrometeor Concentration Measurements," AFGL-TR-76-0187 (13 August 1976). AD-A032 311

Concentration factor is determined by computing particle trajectories from the free stream (initial plane in Fig. 5) to a small area in the target plane (Fig. 5) that surrounds the target point such as to define a particle flux tube. Since the particle mass transfer rate through the tube is constant at all cross sections, it is easily shown that

$$C_F \simeq \frac{A}{A_t} \quad , \tag{3}$$

where A and A_t are the flux tube cross sectional areas in the free stream and at the target point. In the limit as A and A_t approach zero, eq. (3) becomes exact.

For the situation considered here the target plane is constrained to lie parallel to the EWER orifice plane at a distance 1.5 mm upstream from it. Target points are defined near the orifice periphery, at 95% of the orifice radius, such that the flux tube incident on the target plane envelopes approximately 90% of the flux into the orifice.

The water content implied by eq. (2) applies only to the EWER orifices; it is not the water content seen by the Lyman-α detector which is located inside the wing pod. This is because air entering a EWER orifice has speed ηV (η = 0.45 in this case) while hydrometeors enter at speed $V_{p,t} > \eta V$. Once inside the EWER tube, however, the hydrometeors are vaporized and henceforth assume the same speed as the air. If we ignore compression effects and recognize that pressure and temperature differences between the detector chamber and ambient are corrected for elsewhere, a simple mass balance shows that the concentration ratio in the detector chamber, $C_{M,E}$ is

$$C_{M,E} = C_F/\eta \ . \tag{4}$$

Thus, while $C_{M,t}$ (eq. (2)) indicates hydrometeor collection efficiency by the EWER, the hydrometeor measurement efficiency is given by eq. (4).

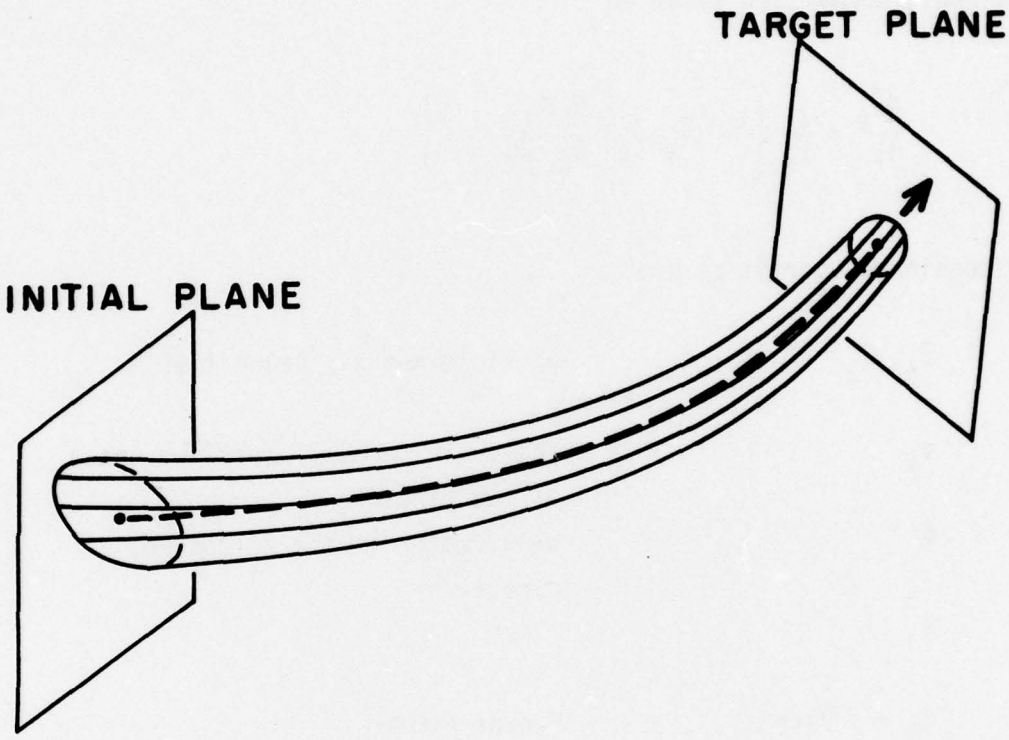

Figure 5. Perspective view of a hydrometeor flux tube. The initial and target planes are perpendicular to the central trajectory (dashed line). Since the peripheral trajectories are constrained to pass through a circle about the central trajectory in the target plane, in general they pass through a non-circular, closed curve in the initial plane.

PARTICLE TRAJECTORY CALCULATION

We assume that the bulk air flow is not perturbed by the particles. Moreover, since particle density is large compared to that of air, we can neglect buoyancy and inertial reaction of the fluid to obtain the three-dimensional, normalized equation

$$\frac{d\vec{v}_p}{d\tau} = \frac{1}{F_N}\left\{\frac{1}{v_s}(\vec{v}_a-\vec{v}_p)\frac{B_N R_{N,s}}{B_{N,s} R_N} - \vec{k}\right\} \tag{5}$$

Non-dimensioned quantities are:

$\vec{v}_p$, $\vec{v}_a$	particle and air velocities
v_s	still-air terminal settling speed of the particle
$\vec{k}$	unit vector in the z (upward) direction
τ	time
$F_N = V^2/(Lg)$	Froude Number
$R_N = \frac{\rho\delta}{\eta}\left\|\vec{v}_a-\vec{v}_p\right\| V$	Reynolds Number
$B_N = C_D R_N^2$	Davies Number
C_D	particle drag coefficient

Dimensioned quantities are:

δ	particle dimension
ρ	air density
η	air viscosity
g	gravity acceleration constant
V	freestream airspeed
L	a characteristic dimension of the fuselage

Here length is normalized by L, velocity by V and time by L/V. $R_{N,s}$ and $B_{N,s}$ are for still-air, terminal settling of the particles.

Starting at the initial plane, eq. (5) is integrated with respect to time in three dimensional space via the code DVDQ of Krogh[5] until the target is reached. The method used to compute $\vec{v}_a$ at each time step is described next, and then drag coefficients are discussed.

THREE-DIMENSIONAL FLOW CALCULATION

In performing concentration factor calculations for sampling sites on particular airplanes, it is important to use three-dimensional airflow. This is the only way to properly account for: airplane geometry and angle-of-attack, airspeed, altitude, and particle settling.

Cloud physics airplanes are subsonic, sampling runs being made typically between 100-150 kts indicated airspeed (IAS). Particle measurement points are beyond the skin-friction boundary layer, and should be placed to avoid regions of separated flow. Therefore,

5. F.T. Krogh, "Variable Order Integrators for Numerical Solutions of Ordinary Differential Equations," Jet Propulsion Lab Technology Utilization Document No. CP-2308 (November 1970).

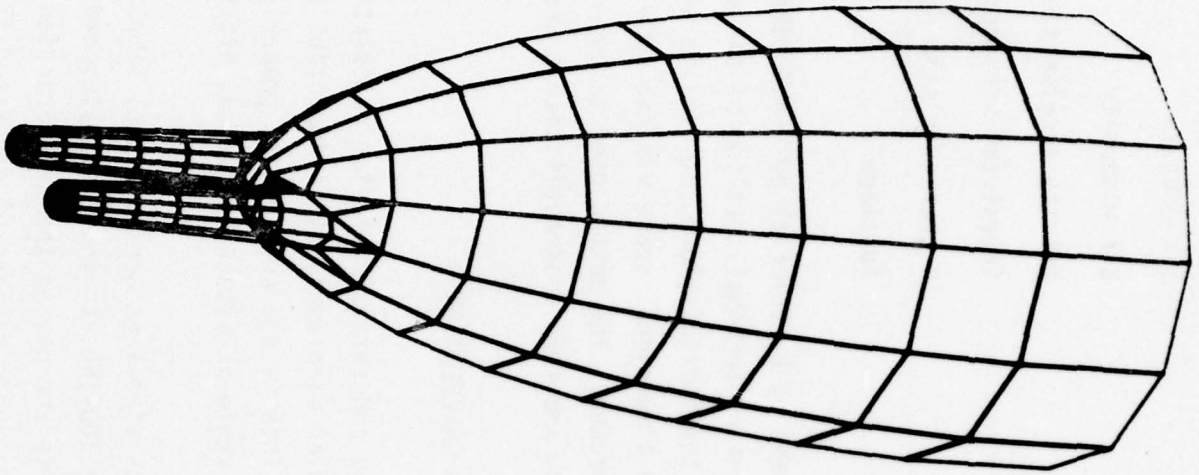

Figure 6. Computer plot of the digital description of the EWER probes and wing pod nose.

potential (i.e., frictionless, incompressible, laminar) flow calculations are quite adequate. We use a code developed by Hess and Smith[6,7] for calculating potential flow about arbitrary three-dimensional bodies. The Hess-Smith code requires input of a digital description of the body surface. This consists of the coordinates of the corner points of a large number of contiguous, plane, quadrilaterals. Figure 6 shows a computer plot of the digital description of the EWER probes and wing pod nose used for this study.

Accuracy of the flow calculations has been checked with excellent results by Hess and Smith[6] for many bodies for which analytical solutions are available. Norment and Zalosh[2] have compared computed trajectories around ellipsoids in analytical flow fields with similar trajectories in Hess-Smith flow fields, and they have compared current trajectory results with prior work; agreement is excellent.

PARTICLE DRAG COEFFICIENT

Davies[8] shows that still-air terminal settling of spheres can be generalized in terms of the dimensionless numbers $R_{N,s}$ and $B_{N,s}$. Over the range from the smallest spheres, which settle under viscous flow conditions and obey Stokes law, to spheres much larger than of interest here, and for any Newtonian fluid, a reproducible single-valued relationship between $R_{N,s}$ and $B_{N,s}$ exists. Furthermore, $B_{N,s}$ is independent of settling speed, being a function of fluid and sphere properties only; thus for given sphere and fluid, $R_{N,s}$ and hence V_s can be calculated. Polynomials by which $R_{N,s}$ can be computed as a function of $B_{N,s}$ were derived by Davies from a composite of many sets of experimental data.

---

6. J.L. Hess and A.M.O. Smith, "Calculation of Non-Lifting Potential Flow About Arbitrary Three-Dimensional Bodies," McDonnel Douglas Report E.S. 40622 (15 March 1962). AD-282 255.

7. J.L. Hess and A.M.O. Smith, "Calculation of Potential Flow About Arbitrary Bodies," Progress in Aeronautical Sciences, Vol. 8, edited by D. Kuchemann (Pergammon Press, New York, 1967).

8. C.N. Davies, "Definitive Equations for the Fluid Resistance of Spheres," Proc. Phys. Soc. (London) 57, 259-270 (1945).

Since the work of Davies, it has been found repeatedly that this treatment is applicable to particles of other shapes, providing settling is steady and particle orientation is stable.

For the trajectory calculations required here, the problem must be turned around. In addition to gravity settling, there is a particle velocity component (relative to air) caused by the disturbance of the passing airplane. At any time step in the numerical integration of eq. (5), $\vec{v}_a - \vec{v}_p$ (and hence R_N) is known, and B_N must be determined. For viscous motion (i.e., Stokes flow, where $R_N < 1$) $B_N = 24\ R_N$ and eq. (5) can be integrated without question. However, for larger R_N the steady-state drag data determined experimentally for terminal settling must be used to compute accelerative particle motion.

Experimental measurements by Keim[9] and a theoretical analysis by Crowe, et al.[10] indicate that if the acceleration modulus,

$$A_N = \delta \left| \frac{dV_p}{dt} \right| / V_p^2 \quad ,$$

is smaller than about 10^{-2}, steady-state drag coefficients can be used without significant error to compute accelerative motion. A_N has never been found to exceed 10^{-2} in our trajectory calculations.

For small water drops, which are spherical, the polynomial equations of Davies[8] are used to compute V_s, while for larger, distorted drops, the equations of Foote and du Toit[11] are used. To compute B_N from R_N, inverse polynomials have been developed, using the data set given by Davies for small drops and Gunn and Kinser[12] for large drops.

---

9. S.R. Keim, "Fluid Resistance to Cylinders in Accelerated Motion," J. Hydraulics Div., Proc. Amer. Soc. Civil Eng., 6, paper 1113 (1956).
10. C.T. Crowe, J.A.Nicholls and R.B. Morrison, "Drag Coefficients of Inert and Burning Particles Accelerating in Gas Streams," Ninth Symp. (Int'l.) on Combustion, Academic Press, pp. 395-405 (1963).
11. G.B. Foote and P.S. du Toit, "Terminal Velocity of Raindrops Aloft," J. Appl. Meteor. 8, 249-253 (1969).
12. R. Gunn and G.D. Kinser, "The Terminal Velocity of Fall for Water Droplets in Stagnant Air," J. Meteor. 6, 243-248 (1949).

Concentration factors also are calculated for five different ice crystal forms and for broad ranges of ice crystal sizes. Tables of ice crystal properties used in this study are presented below in Tables 2 through 5.

CALCULATION DETAILS

EWER DIGITAL DESCRIPTION AND FLUX TUBE GEOMETRY

The digital description shown in Fig. 6 was developed from half-scale engineering drawings. Coordinate measurements are accurate to about one millimeter. As shown in Fig. 7 the EWER orifice plane is defined by twenty-one quadrilaterals. Each of these quadrilaterals is required to leak inward 45% of the free stream flow. Flow into and around the orifice is shown in Fig. 8.

The target plane used to calculate concentration factors is parallel to the orifice plane and offset from it in the downstream direction by 1.5 mm. The purpose of the offset is to avoid direct contact with quadrilateral edge, corner and gap discontinuities.

Hydrometeor flux tubes are defined by seven trajectories for all cases: one trajectory to the center of the orifice plus six equally spaced around its periphery at distances from the center of 95% of the orifice radius. Trajectories to these specified points were calculated by the iterative method described by Norment and Zalosh.[2] Figures 9 and 10 illustrate trajectory flux tubes for large and small hydrometeors respectively.

FLIGHT CONDITIONS

Indicated airspeed of 150 knots with 4° angle-of-attack,* nose up, were assumed for all cases, and calculations were done for three altitudes: 2 km, 5 km, and 7.5 km relative to sea level. Atmospheric conditions at these altitudes were taken from the U.S. Standard Atmosphere, 1962[13] and are presented in Table 1 along with true airspeeds.

HYDROMETEOR PROPERTIES

Selection and analysis of hydrometeor drag and dimension data are discussed in detail in refs. 2 and 3. Ice hydrometeor properties are presented here in Tables 2 through 5. In the trajectory calculations the

* The 4° angle-of-attack is somewhat arbitrary in that the actual angle varies slightly with altitude, load weight and other flight conditions, but small changes in the angle would be expected to have minor effects on the results.

13. S. L. Valley, Editor, Handbook of Geophysics and Space Environments, (McGraw-Hill, 1965).

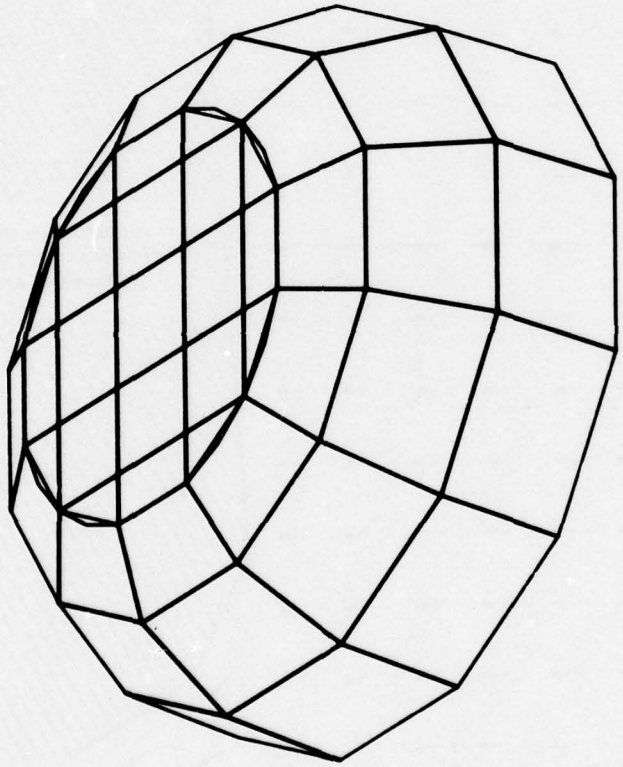

Figure 7. Computer plot of tip and orifice of a EWER probe.

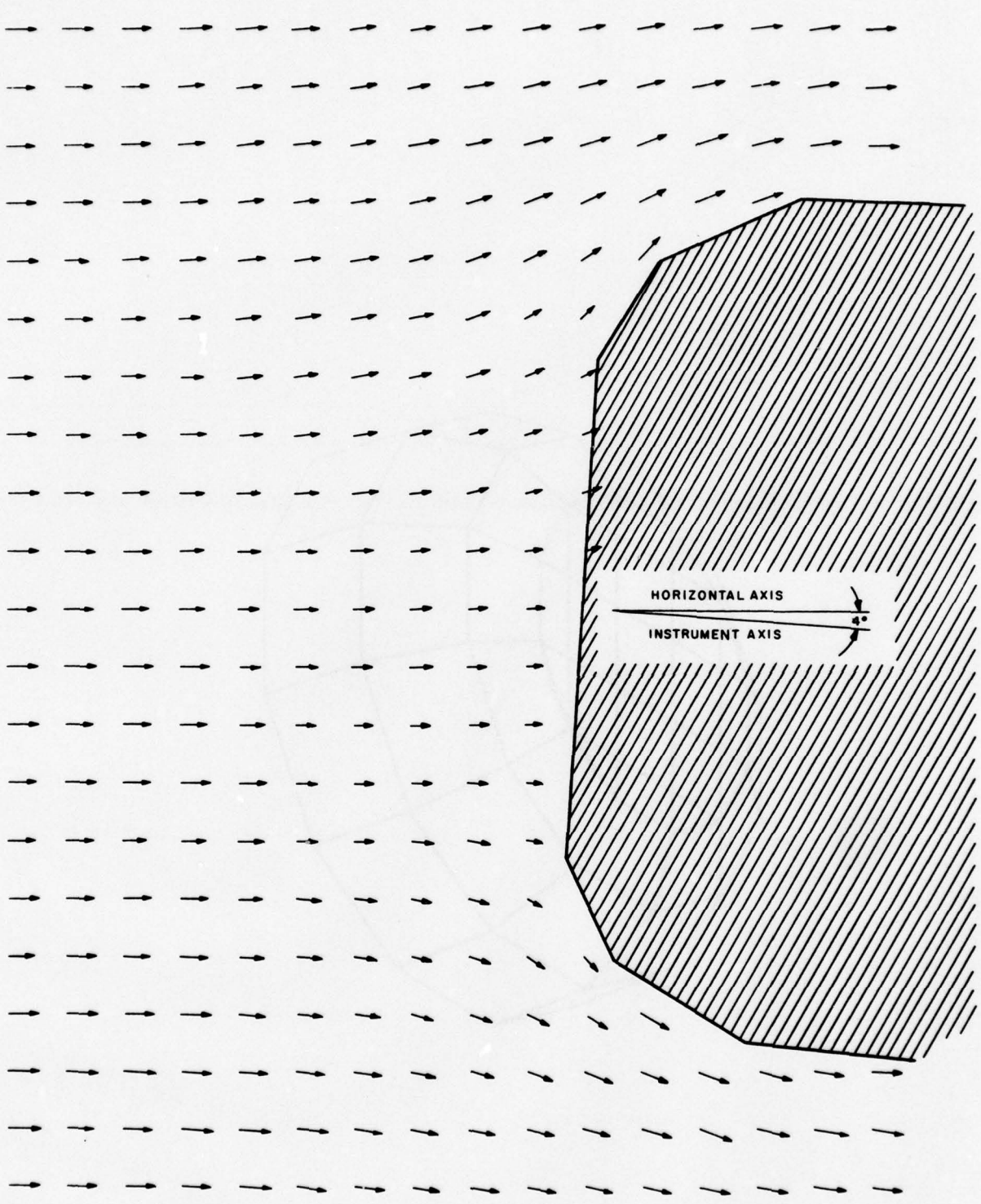

Figure 8. Airflow vectors in the vertical plane through the center of the EWER orifice.

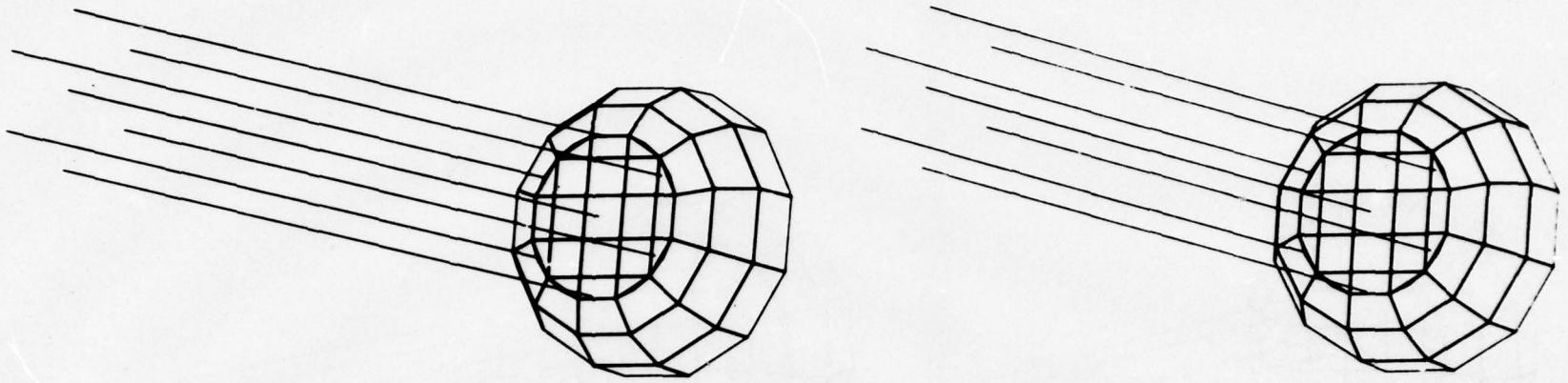

Figure 9. Stereo view of 1000 μm water drop trajectories into the EWER orifice. Three-dimensional perspective can be attained by staring at the center of the figure and then crossing the eyes such that the two images merge.

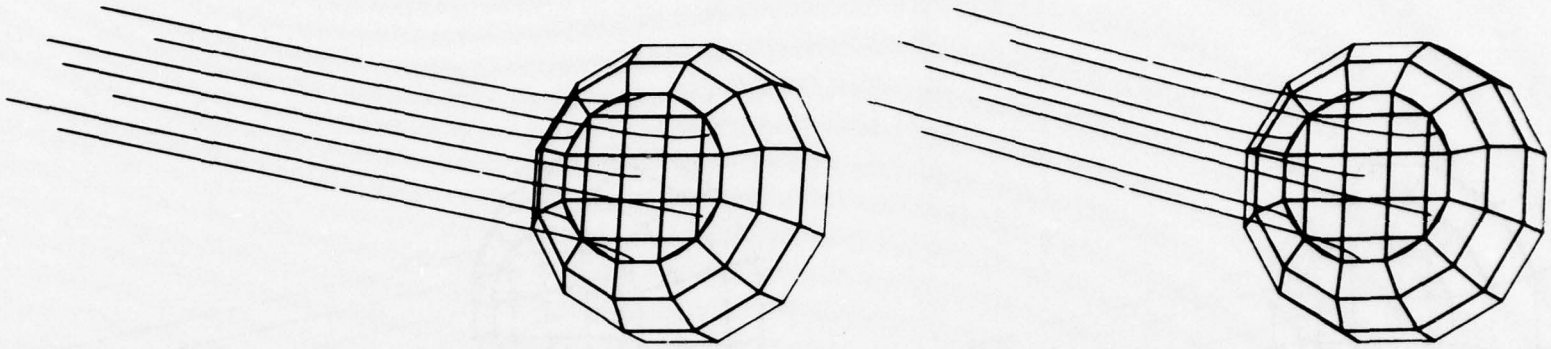

Figure 10. Stereo view of 20 μm long hollow ice column trajectories into the EWER orifice. (See Table 2 for ice column properties.) Three-dimensional perspective can be attained by staring at the center of the figure and then crossing the eyes such that the two images merge.

TABLE 1

ATMOSPHERE PROPERTIES AND TRUE AIRSPEEDS

Altitude (km RMSL)	Temperature (^{o}K / ^{o}C)	Pressure (Pa)	Density (kg/m^3)	True Airspeed (m/s)
2	275.15 / 2.00	79501	1.0066	86.75
5	255.68 / -17.47	54048	0.7364	101.03
7.5	239.46 / -33.69	38378	0.5579	115.51

TABLE 2

PROPERTIES OF COLUMNAR ICE CRYSTALS

Length, ℓ (μm)	Width, δ (μm)	δ/ℓ	Solid Columns*		Hollow Columns*	
			Mass (μg)	Diameter of water drop of equal mass (μm)	Mass (μg)	Diameter of water drop of equal mass (μm)
20	11.559	.578	.001215	13.2	.0006248	10.6
30	17.441	.581	.004149	19.9	.002134	16.0
50	35.8	.715	.0291	38.1	.0149	30.6
100	68.3	.683	.212	74.0	.1091	59.3
300	117.0	.390	1.87	152.8	.960	122.4
500	144.5	.289	4.75	208.5	2.441	167.1
1000	197.3	.197	17.7	323.3	9.100	259.0
3000	310.9	.1036	131.9	631.5	67.82	506.0

*Solid column density is taken to be 0.7 g/cm^3, and hollow column density is taken to be 0.36 g/cm^3.

TABLE 3

PROPERTIES OF HEXAGONAL PLATE (P1a) ICE CRYSTALS

Diameter (μm)	Thickness (μm)	Mass (μg)	Diameter of Water Drop of Equal Mass (μm)	Density (kg/m^3)
10	5.68	$\sim 2.582 \times 10^{-4}$	$\sim$ 7.9	$\sim$ 700.
30	9.30	$\sim 3.591 \times 10^{-3}$	$\sim$ 19	$\sim$ 660.6
50	11.70	$\sim 9.203 \times 10^{-3}$	$\sim$ 26	$\sim$ 484.0
100	15.97	$\sim 3.351 \times 10^{-2}$	$\sim$ 40	$\sim$ 323.0
300	26.16	0.4779	97	312.5
500	32.90	2.145	160	401.5
1000	44.91	20.22	338	693.1

TABLE 4

PROPERTIES OF PLANE DENDRITIC (Ple) ICE CRYSTALS

Dendrite Diameter (μm)	Thickness (μm)	Mass (μg)	Diameter Of Water Drop Of Equivalent Mass (μm)	Equivalent Plate Density (kg/m^3)	Equivalent Plate Diameter (μm)
500	29.16	0.7366	112	334	341.0
600	31.24	1.0980	128	357	389.4
800	34.82	2.1850	161	402	490.3
1000	37.87	3.6484	191	450	574.1
1500	44.13	8.2890	251	556	720.8
1800	47.27	11.494	280	607	785.4
2500	53.50	~ 21.129	~ 343	~ 712	924.1

TABLE 5

PROPERTIES OF AGGREGATES OF UNRIMED RADIATING ASSEMBLAGES OF PLATES, SIDE PLANES, BULLETS AND COLUMNS

Dimension (μm)	Mass (μg)	Density (kg/m^3)	Diameter of Water Drop of Equivalent Mass (μm)
300	3.756	265.7	193
500	9.914	151.5	266
800	24.21	90.3	359
1000	37.0	70.7	413
2000	138.1	33.0	641
3000	298.3	21.1	829

hydrometeors are allowed to settle at their terminal gravity speeds. We assume that columns and plates always orient such that the drag vector is normal to the long axes of the columns and normal to the faces of the plates. These are considered to be good assumptions for this study.

RESULTS

Results are presented in Tables 6 - 10 and $C_{M,E}$ vs. hydrometeor mass is plotted in Fig. 11. Comparison of Figs. 9 and 10 against Fig. 8 illustrates that the smaller particles tend to follow the air flow whereas the larger particles substantially ignore the air flow. Thus, while the larger particles enter the EWER orifices at nearly free stream speeds and at essentially free stream concentrations (see the $V_{p,t}/V$ and $C_{M,t}$ columns in Tables 6 - 10), after vaporization their concentrations approach the limiting value of free stream concentration divided by η (i.e., the heavy particle asymptote in Fig. 11). Since the smaller particles tend to follow the air flow, their concentrations at the orifices also deviate only slightly from free stream values. However, since they enter the orifices at substantially less than free stream speeds, their concentrations after vaporization also are less as shown by their $C_{M,E}$ values, which in the limit of infinitesimal particle mass should approach unity.

Durran, et al.[1] calculated collection efficiencies for several sizes of water drops for several air flux efficiencies for atmospheric conditions at 6.1 km altitude. Their case that matches one of ours closest is for 20 μm diameter drops with $\eta = 0.6$. They present graphs of particle flux and concentration across the orifice; values given here are approximate averages:

	C_F	$C_{M,t}$
Durran et al.[1]	∿ 1.06	∿ 0.85
This study	1.04	0.84

Considering that our calculation was done for 5 km altitude and for $\eta = 0.45$, the agreement is probably good.

TABLE 6

WATER DROP CONCENTRATION RATIOS IN THE EWER

Results are given for three altitudes in the sequence: 2 km, 5 km, 7.5 km

Water Drop Diameter (μm)	Mass (μg)	$V_{p,t}/V^*$	$C_{M,t}$	$C_{M,E}$
	[illegible]	0.626	1.070	1.489
10	5.236×10^{-4}	0.655	1.068	1.554
		0.682	1.064	1.613
		0.777	1.048	1.808
20	4.189×10^{-3}	0.804	1.041	1.861
		0,827	1.036	1.904
		0,847	1.035	1.947
30	.01414	0.869	1.029	1.987
		0.886	1.024	2.018
		0.909	1.023	2.066
50	.06545	0.924	1.018	2.089
		0.936	1.013	2.107
		0.945	1.012	2.126
80	.2681	0.954	1.009	2.140
		0.961	1.006	2.150
		0.957	1.009	2.144
100	.5236	0.964	1.006	2.155
		0.969	1.004	2.162
		0.983	1.000	2.184
300	14.14	0.985	0.999	2.187
		0.987	0.998	2.189
		0.987	0.998	2.191
500	65.45	0.988	0.998	2.192
		0.989	0.998	2.193
		0.990	0.998	2.195
800	268.1	0.990	0.998	2.196
		0.991	0.997	2.196
		0.991	0.997	2.196
1000	523.6	0.991	0.997	2.197
		0.992	0.997	2.197

*$V_{p,t}/V$ here and in Tables 7 - 10 is calculated at a point 1.5 mm upstream of the orifice center. The airspeed ratio at this point is about 0.49 compared with 0.45 in the orifice plane.

TABLE 7

ICE COLUMN CONCENTRATION RATIOS IN THE EWER

Results are given for three altitudes in the sequence: 2 km, 5 km, 7.5 km

Column Length* (μm)	Solid Columns			Hollow Columns		
	$V_{p,t}/V$	$C_{M,t}$	$C_{M,E}$	$V_{p,t}/V$	$C_{M,t}$	$C_{M,E}$
	0.644	1.072	1.535	0.576	1.056	1.353
20	0.670	1.071	1.595	0.594	1.062	1.402
	0.694	1.067	1.647	0.611	1.066	1.447
	0.723	1.077	1.729	0.642	1.087	1.550
30	0.753	1.068	1.788	0.670	1.083	1.612
	0.780	1.060	1.836	0.695	1.078	1.666
	0.839	1.050	1.957	0.768	1.073	1.830
50	0.864	1.041	1.998	0.799	1.061	1.884
	0.883	1.034	2.030	0.824	1.052	1.928
	0.908	1.030	2.079	0.858	1.049	2.001
100	0.925	1.023	2.103	0.882	1.040	2.037
	0.938	1.018	2.120	0.900	1.032	2.065
	0.946	1.016	2.137	0.914	1.030	2.092
300	0.957	1.011	2.150	0.930	1.023	2.114
	0.964	1.008	2.160	0.942	1.018	2.130
	0.957	1.012	2.152	0.930	1.024	2.116
500	0.965	1.008	2.162	0.943	1.018	2.134
	0.971	1.005	2.169	0.953	1.013	2.146
	0.968	1.007	2.166	0.948	1.016	2.142
1000	0.974	1.004	2.173	0.958	1.011	2.154
	0.978	1.002	2.178	0.965	1.008	2.163
	0.978	1.002	2.179	0.966	1.008	2.165
3000	0.982	1.001	2.183	0.972	1.005	2.172
	0.984	1.000	2.186	0.977	1.003	2.177

*See Table 2 for ice column properties.

TABLE 8

HEXAGONAL PLATE (P1a) CONCENTRATION RATIOS IN THE EWER

Results are given for three altitudes in the sequence: 2 km, 5 km, 7.5 km

Plate Diameter* (μm)	$V_{p,t}/V$	$C_{M,t}$	$C_{M,E}$
	0.643	1.062	1.518
10	0.676	1.060	1.594
	0.708	1.056	1.661
	0.718	1.075	1.715
30	0.750	1.067	1.779
	0.779	1.059	1.833
	0.733	1.078	1.756
50	0.764	1.069	1.817
	0.792	1.061	1.867
	0.753	1.083	1.812
100	0.784	1.073	1.869
	0.811	1.063	1.916
	0.842	1.062	1.986
300	0.869	1.050	2.027
	0.890	1.040	2.058
	0.890	1.043	2.064
500	0.911	1.033	2.092
	0.926	1.026	2.112
	0.945	1.019	2.140
1000	0.956	1.013	2.153
	0.964	1.009	2.162

*See Table 3 for properties of hexagonal plates.

TABLE 9

PLANE DENDRITE (P1e) CONCENTRATION RATIOS IN THE EWER

Results are given for three altitudes in the sequence: 2 km
5 km
7.5 km

Dendrite* Diameter (μm)	$V_{p,t}/V$	$C_{M,t}$	$C_{M,E}$
	0,861	1.053	2.016
500	0.886	1.042	2.052
	0.904	1.034	1.079
	0.895	1.040	2.070
800	0.915	1.031	2.096
	0.930	1.024	2.116
	0.910	1.035	2.092
1000	0.927	1.026	2.114
	0.940	1.020	2.131
	0.940	1.020	2.133
1800	0.952	1.015	2.148
	0.961	1.011	2.158
	0.952	1.015	2.148
2500	0.962	1.010	2.160
	0.968	1.007	2.167

*See Table 4 for plane dendrite properties.

TABLE 10

CRYSTAL AGGREGATE CONCENTRATION RATIOS IN THE EWER

Results are given for three altitudes in the sequence: 2 km, 5 km, 7.5 km

Aggregate Dimension* (μm)	$V_{p,t}/V$	$C_{M,t}$	$C_{M,E}$
	0.970	1.003	2.162
300	0.974	1.001	2.169
	0.978	1.000	2.174
	0.975	1.001	2.170
500	0.978	1.000	2.175
	0.981	0.999	2.179
	0.978	1.000	2.175
800	0.981	0.999	2.179
	0.983	0.999	2.182
	0.980	1.000	2.177
1000	0.982	0.999	2.181
	0.984	0.998	2.184
	0.983	0.999	2.183
2000	0.985	0.998	2.186
	0.986	0.998	2.187
	0.985	0.998	2.186
3000	0.986	0.998	2.188
	0.988	0.998	2.189

*See Table 5 for crystal aggregate properties.

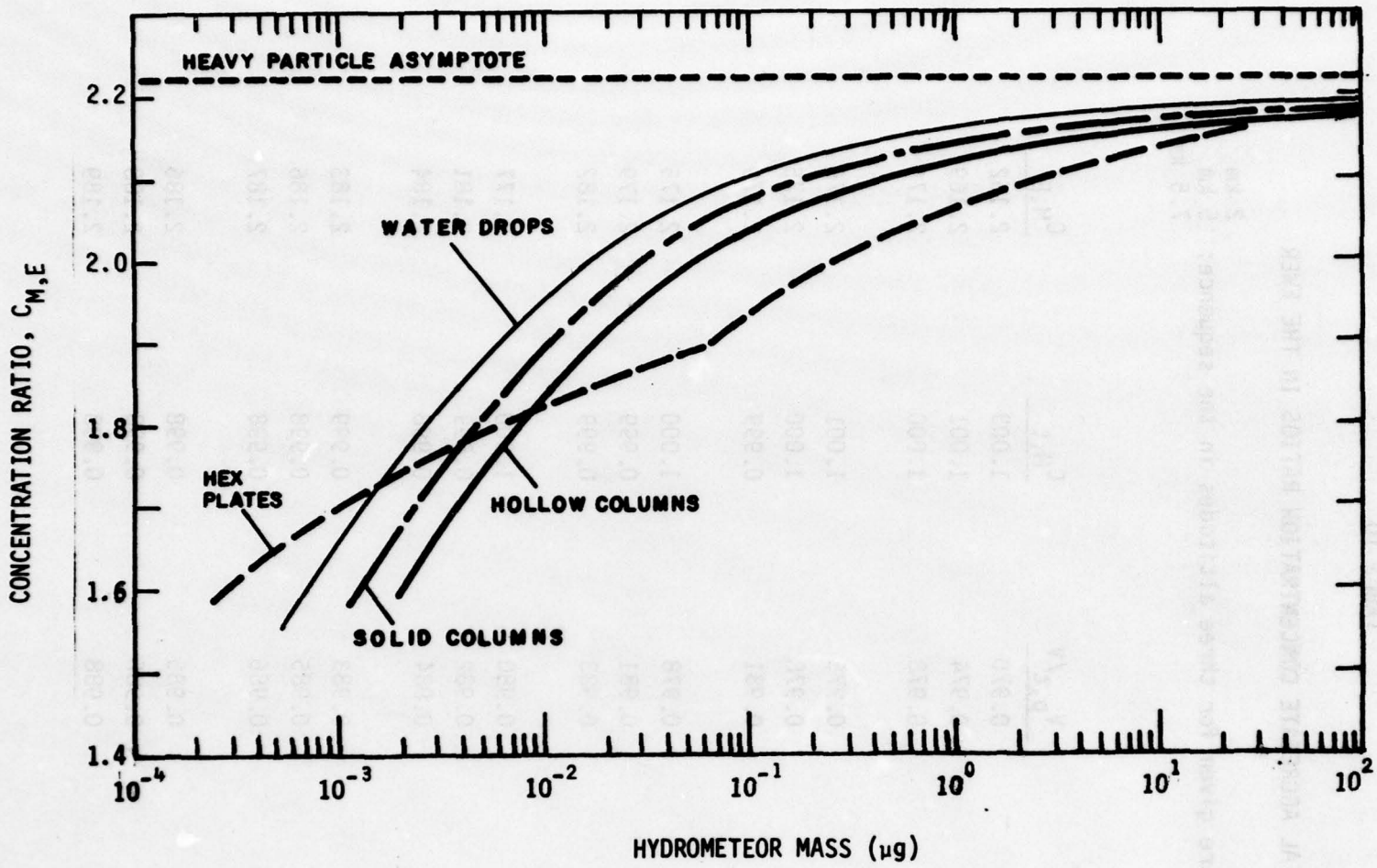

Figure 11. Concentration ratio vs. particle mass for various hydrometeors at 5 km altitude. For the heavy particle asymptote, $C_{M,E} = \eta^{-1} = 2.222$. Tables 2-6 list particle masses for the hydrometeors studied. Data for plane dendrites and aggregates are not included since they fall between the curves shown on the already crowded right-hand side of the graph.

From Fig. 11 and Tables 6 - 10 we see that the largest deviation of concentration ratio from the heavy particle limit is about ten percent for particles heavier than 0.5 μg. For smaller particles, the concentration ratio falls away from the heavy particle limit toward unity, with the smallest value calculated being 1.35 for the case of hollow columns of 20 μm length at 2 km altitude.

REFERENCES

1. D. A. Durran, D. H. Ross and W. J. Swartwood, "Development of Cloud Water Content Meter, EWER," The Aerospace Corp., Report SAMSO-TR-78-113 (March 1978). AD-A061 255

2. H. G. Norment and R. G. Zalosh, "Effects of Airplane Flowfields on Hydrometeor Concentration Measurements," AFCRL-TR-74-0602 (6 December 1974). AD-A006 690

3. H. G. Norment, "Effects of Airplane Flowfields on Cloud Water Content Measurements," AFCRL-TR-75-0231 (30 April 1975). AD-A014 807

4. H. G. Norment, "Additional Studies of the Effects of Airplane Flowfields on Hydrometeor Concentration Measurements," AFGL-TR-76-0187 (13 August 1976). AD-A032 311

5. F. T. Krogh, "Variable Order Integrators for Numerical Solutions of Ordinary Differential Equations," Jet Propulsion Lab Technology Utilization Document No. CP-2308 (November 1970).

6. J. L. Hess and A.M.O. Smith, "Calculation of Non-Lifting Potential Flow About Arbitrary Three-Dimensional Bodies," McDonnel Douglas Report E.S. 40622 (15 March 1962). AD-282 255.

7. J. L. Hess and A.M.O. Smith, "Calculation of Potential Flow About Arbitrary Bodies," Progress in Aeronautical Sciences, Vol. 8, edited by D. Kuchemann (Pergammon Press, New York, 1967).

8. C. N. Davies, "Definitive Equations for the Fluid Resistance of Spheres," Proc. Phys. Soc. (London) 57, 259-270 (1945).

9. S. R. Keim, "Fluid Resistance to Cylinders in Accelerated Motion," J. Hydraulics Div., Proc. Amer. Soc. Civil Eng., 6, paper 1113 (1956).

10. C. T. Crowe, J. A. Nicholls and R. B. Morrison, "Drag Coefficients of Inert and Burning Particles Accelerating in Gas Streams," Ninth Symp. (Int'l.) on Combusion, Academic Press, pp. 395-405 (1963).

11. G. B. Foote and P. S. du Toit, "Terminal Velocity of Raindrops Aloft," J. Appl. Meteor. 8, 249-253 (1969).

12. R. Gunn and G. D. Kinser, "The Terminal Velocity of Fall for Water Droplets in Stagnant Air," J. Meteor. 6, 243-248 (1949).

13. S. L. Valley, editor, Handbook of Geophysics and Space Environments, (McGraw-Hill, 1965).